# AUTOMATED EXTRACTION OF CORONARY ARTERY CENTERLINES FROM CT ANGIOGRAPHY IMAGES USING CYLINDRICAL TEMPLATE MATCHING

A Thesis

Presented to the Faculty of the Graduate School

of Cornell University

in Partial Fulfillment of the Requirements for the Degree of

Master of Science

by

Sergei Victorovich Fotin

May 2010

## ABSTRACT

Recent developments in computed tomography angiography (CTA) imaging allow for the acquisition of contrast-enhanced volumetric images of the human heart region. High resolution CTA images are vital in obtaining precise information about the structure of the coronary arteries and help to make more accurate clinical diagnosis of coronary heart disease. This work is focused on an automated method for the reconstruction of individual coronary artery centerlines.

An algorithm to automatically identify the centerlines of coronary arteries in a three-dimensional CTA image set based on local tubular matching was developed. The algorithm is seeded with manually specified starting points at the distal location of a coronary artery and then proceeds iteratively toward the junction with the aorta. The algorithm makes necessary corrections to account for motion artifacts and is able to perform on the images of moderately diseased arteries.

Twelve cardiac CTA cases were used for algorithm validation. For each case, the four longest visually discernible branches of the major coronary arteries were evaluated. For 85% of these branches, the algorithm was able to extract the entire centerline automatically from a single manual initialization. In addition, the geometric accuracy of the reconstruction was evaluated by measuring the distance between automatically extracted and manually marked centerlines. For the five artery segments used in this study, the average distance between

the centerlines did not exceed 0.70 mm with the maximum distance of 2.15 mm. These results indicate that the suggested method can be successfully used to approach the goal of automated coronary artery segmentation.

## BIOGRAPHICAL SKETCH

Since 2005, Sergei Fotin has been working with the Vision and Image Analysis Research Group at Cornell University. Prior coming to Cornell, he studied at Ural State Technical University, Yekaterinburg, Russia, in the Division of Radioengineering, and received his degree in 2003 with a major in Software and Computer Engineering. He also used to work as a developer at software engineering firms in Russia.

## ACKNOWLEDGEMENTS

I would like to thank my academic adviser, Anthony Reeves, for the major support and assistance in this research work; Peter Doerschuk and Noah Snavely for serving as my special committee members; Matt Cham for providing patient CTA data; Avital Mendelson and Dong June Song for the assistance during the initial phase of this project; and, finally, my research colleagues Alberto Biancardi, Andy Browder, Eric Heinz, Artit Jirapatnakul, Brad Keller, Jaesung Lee, Jeremiah Wala for help, support and being good friends at the same time.

## TABLE OF CONTENTS

## LIST OF FIGURES

## LIST OF TABLES

CHAPTER 1

# INTRODUCTION

Coronary artery disease is the condition when the myocardium blood supply is reduced or stopped because of a blockage of a coronary artery. The disease usually starts with atherosclerosis, the buildup of a fatty plaque on the inner artery walls. This plaque may grow or be displaced resulting in a clot blocking the normal blood flow. If the corresponding heart muscle does not receive enough blood oxygen, it leads to ischemia or, in severe cases, to myocardial infarction, which is commonly referred to as the heart attack.

Coronary heart disease is the leading cause of human death worldwide with the highest prevalence in developed countries. According to the United States studies of National Heart, Lung and Blood Institute [1], an estimated 770,000 people had a new coronary attack and about 430,000 had a recurrent attack in year of 2008. There is a number of silent heart attacks occur in addition to the registered cases. The data from National Center for Health Statistics [2] suggests that the disease caused 451,326 deaths in 2004 which was approximately one of every five deaths in the United States.

There are multiple ways for assessing the severity of this disease. The conventional diagnosis method is invasive coronary angiography, which provides two-dimensional X-ray projection images of target blood vessels. However, recent developments in cardiac computed tomography angiography (CTA) allow physicians to obtain three-dimensional high-resolution images of coro-

[1] National Heart, Lung, and Blood Institute, `http://www.nhlbi.nih.gov/`
[2] National Center for Health Statistics, `http://www.cdc.gov/nchs/`

nary arteries and make more qualified assessment of the disease [Kopp et al., 2004; Thompson and Stanford, 2005]. In addition, CTA is a less expensive procedure and carries less risk to the patient. With the large volumes and three-dimensional character of CTA data to process, the demand for computer-assisted analysis methods is growing.

## 1.1 Problem statement

The diagnostic process for coronary heart disease involves examining a CTA image of the patient's heart and locating the major branches of the coronary arteries. In clinical practice, an expert visually traces each branch to identify the abnormalities in the shape of the lumen that would indicate the presence of the disease. Then, based on the extent and the character of these abnormalities, the diagnosis is made.

To simplify the evaluation of a single vessel with respect to the disease, it is convenient to have its geometric description. The centerline, or the set of medial points of the vessel cross sections, is one method of describing the structure of the artery. Once the centerline is identified, it is simple to visualize and characterize the artery in a variety of ways. This geometric description may serve as the basis for further shape processing and analysis algorithms. Given the centerline, one may obtain topological and volumetric representation of the vessel [Tyrrell et al., 2007; Wong and Chung, 2006; Yim et al., 2001], analyze the distribution of the image intensities, the variations of cross-sections and other morphological features of the artery that are useful in evaluation of the disease

[Dehmeshki et al., 2007; Maintz et al., 2003]. In addition, the centerline may serve as the path for fly-through visualization of internal volume of coronary arteries [Schroeder et al., 2002; van Ooijen et al., 2007], which is commonly used procedure in clinical practice.

In this thesis, the focus was done on the design and evaluation of automated method that aids the reconstruction of a coronary artery centerline from a cardiac CTA image. It is important to discriminate between the problem of centerline extraction and the problem of vessel segmentation. Although both have the ultimate goal to facilitate the diagnosis of coronary heart disease, the process of segmentation seeks to obtain volumetric representation of the vessel lumen instead of a centerline representation. The technical approaches as well as methods for quality evaluation for these two problems are also different. However, it is possible to obtain a centerline from a volumetric representation by using skeletonization techniques.

## 1.2 Coronary CT angiography

Coronary CT angiography is a variation of computer tomography technique that allows for the acquisition of enhanced three-dimensional images of coronary arteries. Coronary CTA is superior to traditional CT for the imaging of coronary arteries: it provides better visibility of the target coronary arteries by using of special contrast agent and reduces the effect heart motion artifacts by employing cardiac gating technique. Comparing to conventional coronary angiography, CTA angiography images are reconstructed in multiple axial planes

forming a three-dimensional representation of the heart region and coronary artery tree.

### 1.2.1 Contrast enhancement

Contrast enhancement of the target blood vessels is an essential part of the CTA imaging. Even though conventional CT can produce high-quality 3D images, they are not very helpful in diagnosis of the coronary heart disease. Since the X-ray attenuation properties of blood and blood vessel walls are very similar to the ones of surrounding muscle tissue (40-60 HU [1]), the coronary arteries have very poor contrast on a regular CT image. Moreover, if the artery diameter is comparable to the CT voxel size, the partial volume effect comes into play and makes the artery images diluted with the background as shown in Figure 1.1.

Prior and during the actual CTA scanning, a special radio-opaque agent is injected into vein of the patient. This increases the radiodensity of the blood to over 200 HU and enhances its visibility. Once this blood reaches the coronary arteries, their lumens become discernible in CT images. Since the walls of the blood vessel are not enhanced, any subsequent analysis of the image is based on only lumen information. Consequently, if the blood flow of an artery is completely blocked, CTA cannot reveal the lumen of the affected part. A sample slice of a CTA image is shown in Figure 1.2 and the same heart region visualized using volume rendering is depicted in Figure 1.3.

[1] The Hounsfield units (HU) measure the X-ray attenuation of a substance.

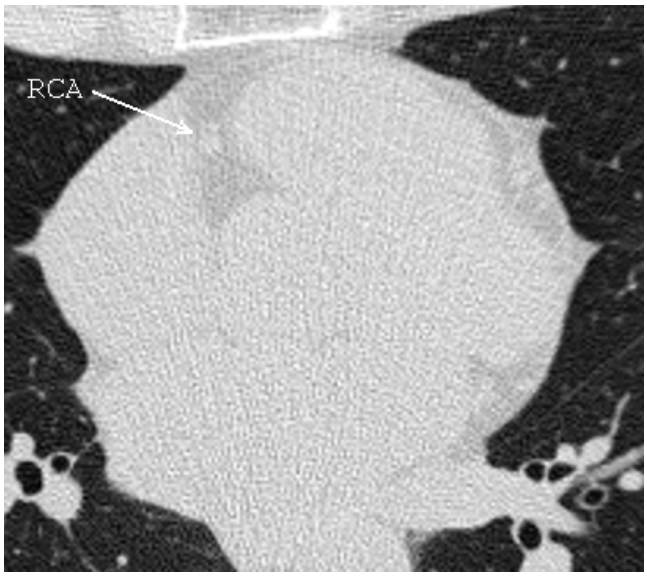


Figure 1.1: Axial slice of a conventional low-dose CT image: profiles of coronary arteries are barely distinguishable from the surrounding tissue. The arrow shows the only profile of right coronary artery that can be recognized.

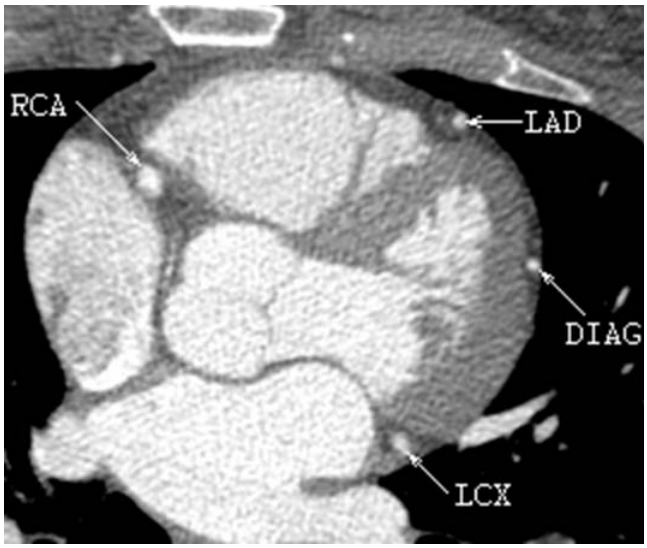


Figure 1.2: Axial slice of a CTA image shows contrast-enhanced lumen profiles of four major branches of the coronary artery: RCA - right coronary artery, LAD - left anterior descending artery, DIAG - its first diagonal branch, LCX - left circumflex artery.

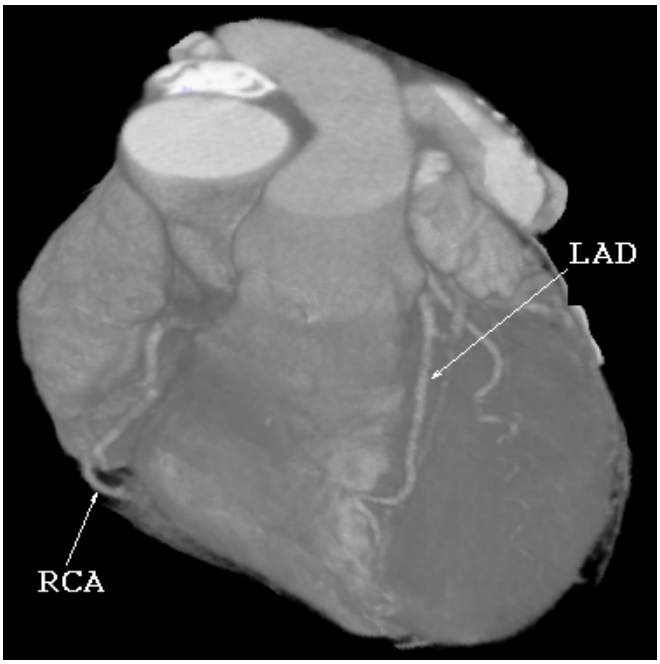


Figure 1.3: Three-dimensional volume rendering of the heart region.

From these images the deviations of shape and morphological abnormalities of an artery such as build-up of a plaque can be captured and evaluated with respect to a condition of the coronary artery. Figures 1.4 and 1.5 illustrate two disease conditions: (a) a coronary artery affected by the calcified plaque and (b) stenosis (narrowing). While calcified plaque may be visible on a regular CT image, soft plaque and stenosis are impossible to diagnose without the CTA contrast enhancement.

## 1.3 CTA gating

Conventional CT imaging substantially affected by the cardiac motion artifacts: modern CT mechanics does not allow snap-shot acquisition of the whole heart

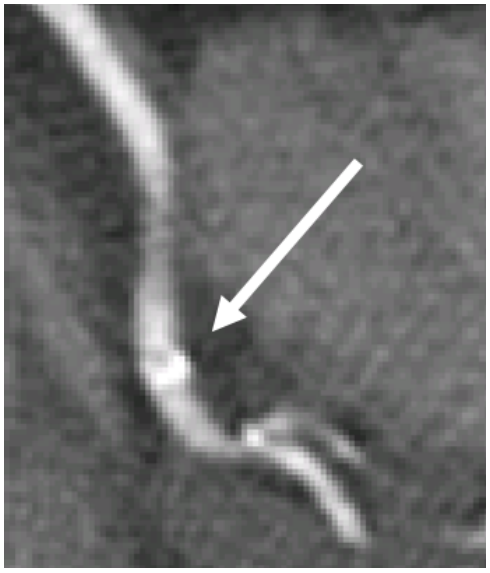

Figure 1.4: Appearance of a plaque in a CTA image: intensity and the shape of the bright spot suggest the presence of a calcification partially blocking the artery.

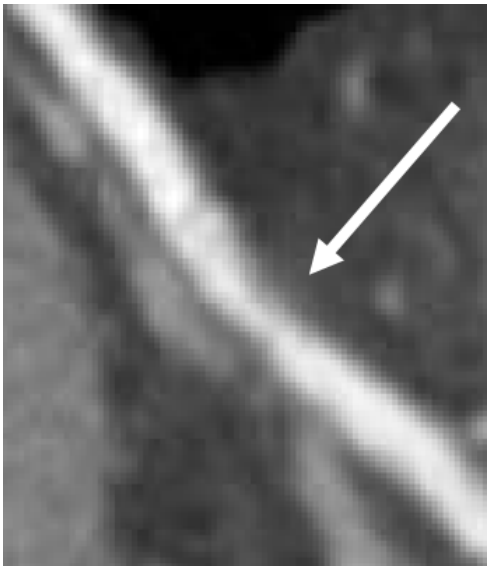

Figure 1.5: Appearance of an artery stenosis (narrowing) in a CTA image: decreased diameter of bright lumen reveals the presence of soft-density plaque on the inner walls of the vessel.

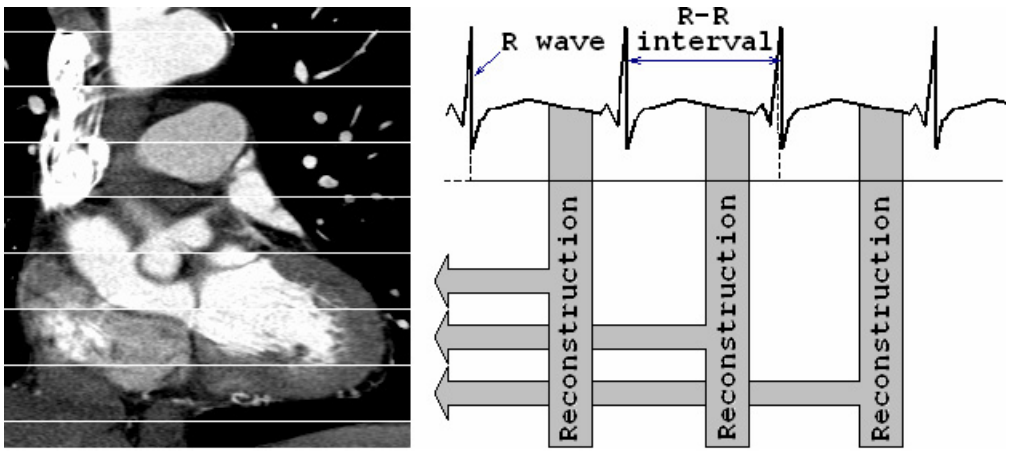


Figure 1.6: Retrospective gating for the acquisition of a cardiac CT image: reconstruction intervals are synchronized with the end-systolic phase of the cardiac cycle as indicated by flat segments of the electrocardiogram signal.

region. Modern 64-slice CT scanners achieve the 360-degree rotation time of 0.3 seconds, while the length of the full heart cycle of 0.8 seconds. Hence, the heart motion during the image acquisition causes blur and periodic displacements and changes in geometry of coronary arteries.

To obtain motionless images of the heart, the technique called ”gating” is applied. The principle of gated acqusition is illustrated in Figure 1.6. Here several consecutive cardiac cycles are used to gather the raw image data as the CT gantry moves along the patient body. Then, given these data and electrocardiogram (ECG) signal taken from a patient, a specialized algorithm is able to reconstruct the image for an arbitrary time phase of the cardiac cycle as if it was taken instantaneously (retrospective gating). Often, the reconstructions are done only for end-systolic phase, when the heart motion is minimized, result in the images of the best quality. To further reduce the impact of increased heart beat rate or cardiac arrhythmia, a patient can be given a beta blocker drug prior

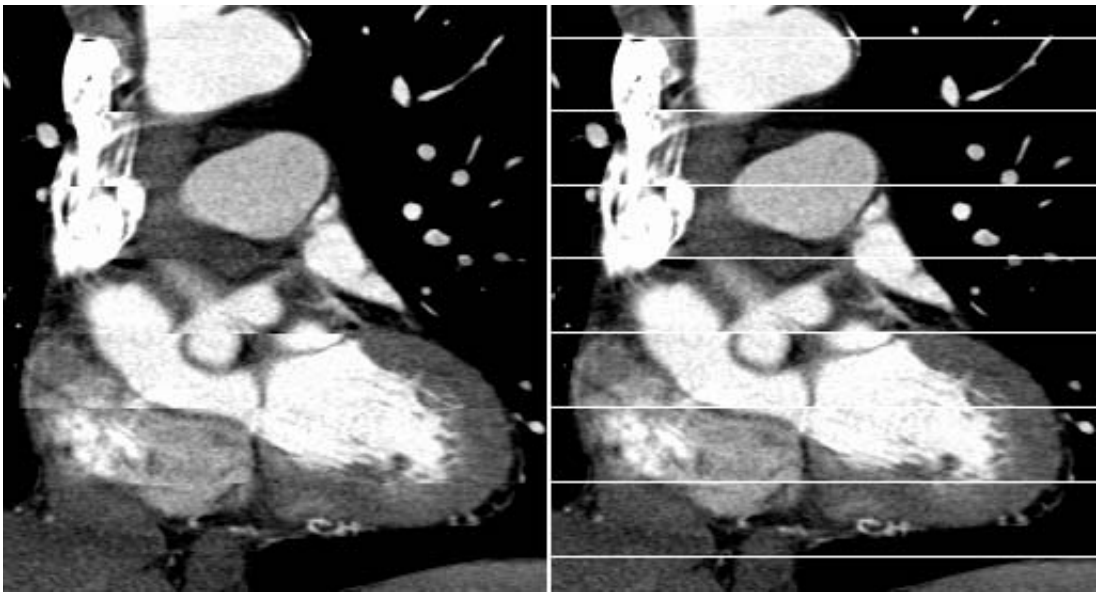

Figure 1.7: Coronal reconstruction of heart region on the left image shows stairstep artifacts. White horizontal lines on the right image denote borders between different cardiac cycles.

to the image acquisition.

However, even for the same phase, heart position may shift slightly between adjacent temporal cycles which causes so-called stairstep artifacts [Lawler et al., 2005]. These artifacts are clearly visible on the coronal image reconstruction shown in Figure 1.7. The impact of the artifacts on the image quality is increased with heart beat rate and degree of arrhythmia that poses a considerable difficulty for automated image analysis methods.

## 1.4 Issues of coronary artery segmentation in CTA image

In addition to heart motion and image reconstruction artifacts, certain features of coronary arteries introduce additional difficulties that must be addressed in the design of an automated centerline extraction method. Anatomically, coronary arteries are narrow blood vessels and when imaged using CTA, appear as thin cylindrical structures of varying curvature. In addition, certain factors may affect the shape and profile of a lument of coronary artery. First, when an artery is affected by atherosclerosis, its lumen may appear as a non-continuous body with a widely varying profile. Second, in case of non-uniform distribution of contrast material, image intensity of the lumen may vary as well.

Figures 1.8 - 1.13 illustrate different issues with appearance of a coronary artery on a cardiac CTA image. Geometric sketches on the left side are supplemented with light shaded three-dimensional visualizations of example coronary artery segments on the right. To obtain each visualization, (a) the 3D region surrounding the artery segment of interest was manually marked and clipped from the image; (b) the intensity threshold of 200 HU was applied to this region; (c) a marching cube algorithm was used to construct a 3D mesh of the artery's boundary; (d) this surface was rendered and captured to the image.

Figure 1.8 shows a typical, relatively straight, segment of a coronary artery that is usually simple to process automatically. The effect of the stairstep artifact that interrupts the continuity of a vessel image is shown in Figure 1.9.

As mentioned earlier, the intensity of the vessel may change due to factors

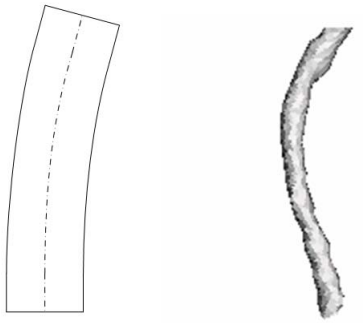

Figure 1.8: A typical segment of a coronary artery.

such as non-uniform distribution of contrast medium, internal calcification and soft plaque. With a change in intensity, a lumen of the artery may be below the threshold value and therefore not be identified as a vessel as illustrated in Figure 1.10. This is the main reason for fixed theshold methods not performing well for coronary artery segmentation.

Besides coronary arteries, a CTA image of the heart may contain various blood regions enhanced by contrast agent. Occasionally, a coronary artery lies very close to another blood vessel or a heart chamber of a similar intensity. Due to partial volume effects, the artery may appear to have ”leaked” into such object as shown in Figure 1.11.

The shape of a coronary artery is often not straight and has a lot of bends and branches. Figure 1.12 shows a sharp turn of a coronary artery that is not peculiar to large blood vessels. Branching points introduce topological problems for almost any centerline extraction methods: it is much easier to process and analyze a straight tube-like structure as opposed to brancing tube structure. Figure 1.13 shows an example of such a bifurcation point.

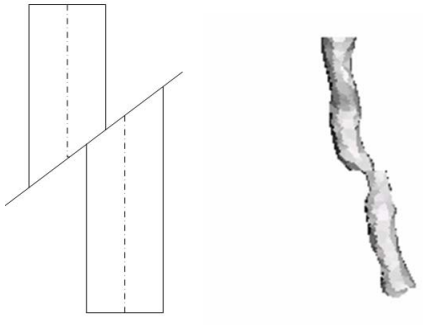

Figure 1.9: Challenge: discontinuity of artery image caused by the stairstep artifact.

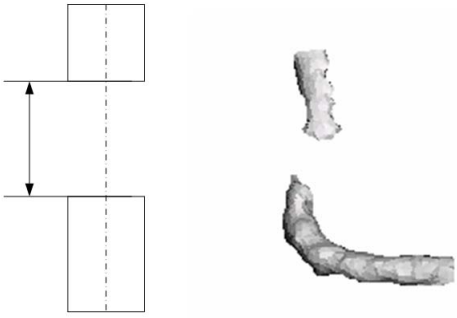

Figure 1.10: Challenge: gap caused by a significant decrease in image intensity (threshold of 200 HU is applied before visualization).

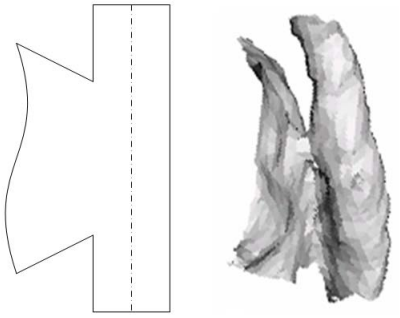

Figure 1.11: Challenge: adjacent structure of high intensity.

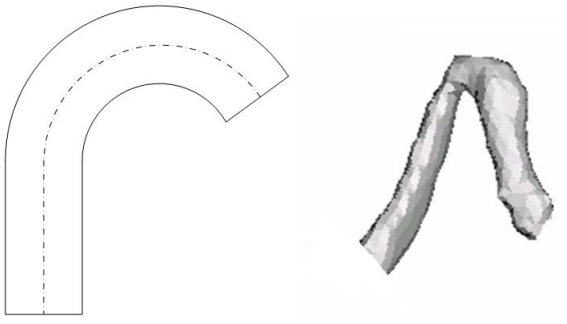

Figure 1.12: Challenge: sharp turn.

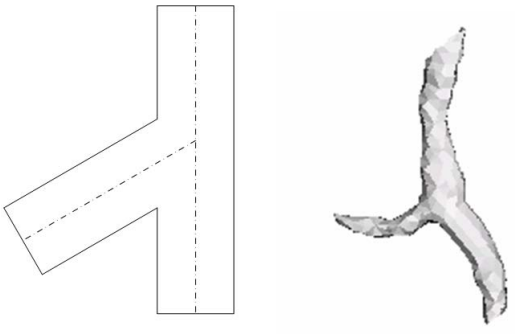

Figure 1.13: Challenge: vessel bifurcation point.

## 1.5 Previous work

There has been a lot of work devoted to the problem of blood vessel centerline extraction. One can find an extensive review of various techniques in works of Bühler et al. [2003] and Kirbas and Quek [2004]. According to the classification of Wink et al. [2000], there are two main types of approaches: indirect and direct. Indirect approaches require certain image preprocessing or presegmentation of a region of interest before the vessel centerline is extracted. In application to coronary arteries, these methods may be based on voxel connectivity [Metz et al., 2007; Ye et al., 2004], morphological filtering [Banh et al., 2007; Mueller et al., 2005], vessel enhancement filtering [Olabarriaga et al., 2003; Yang,

2007] and many other techniques. After initial preprocessing has been done, the centerline is obtained by using skeletonization methods such as thinning [Lam et al., 1992] and medial axis transform [Blum, 1967].

Direct approaches are less constrained since they interact with the image data directly and do not depend on underlying methods. Usually these methods are based on tubular models and exploit the geometrical properties of a blood vessel [Krissian et al., 2000; Tyrrell et al., 2007; Wink et al., 2000]. Among the methods applied the problem of coronary artery segmentation are front propagation [Lavi et al., 2004], local moments from tubular structures [Boldak, 2003] and modeling of vessels as four-dimensional curves [Li and Yezzi, 2007].

If one looks at the problem of vessel centerline extractions from optimization standpoint, all the methods may be classified into either local or global. Local methods seek to obtain the structure of the coronary artery tree in a sequential manner, where the segments of the tree are reconstructed iteratively one by one based on already extracted parts. Global methods, in contrast, try to find the optimal coronary artery path at once, usually using graph-based optimization techniques.

An example of a local method is presented by Wink et al. [2000]. An operator has to define two seed points that initialize the vessel tracking procedure. At each step of the tracking procedure the next point of the centerline is determined from the plane constructed perpendicular to an axis, obtained in the previous step. This plane is examined for the presence of the blood vessel profile and the center point is estimated using ray casting followed by special likelihood

measure. Then, the centerline is adapted based on newly obtained information and so on. This algorithm demonstrated visually acceptable results on the images of the abdominal aorta obtained using different modalities: CTA and Magnetic Resonanse Angiography (contrast enhanced and phase contrast). For CTA modality, in 22 cases out of 26, the aorta was delineated using just seed points without additional user interaction. In the remaining four cases, an operator had to step in to correct the tracking process.

Yang [2007] presented a local algorithm for segmenting coronary arteries from CTA using evolving active contour models. This is an indirect approach that requires heart region presegmentation and vessel image enhancement. Major part of this work has been devoted to volumetric segmentation and concentrated rather on obtaining an accurate representation of the artery surface than on defining the coronary tree structure. The method is fully automated and produced visually plausible results on eighteen clinical cases. Evaluation of the segmentation quality was determined from the comparison of automatically and manually marked artery volumes. Sensitivity of the algorithm varied from 80.69% to 97.88%, while the specificity was in range from 87.77% to 98.95%. Centerline extraction was done as post-processing given the volume is segmented. Quantitative evaluation of centerlines extraction has been done only for digital phantoms, while the real clinical cases were evaluated subjectively.

Olabarriaga et al. [2003] presented a global optimization approach for tracking of coronary arteries from cardiac CTA images. First, the graph cost map was constructed based on second-order properties of image intensity that indicate the likelihood of vessel presence on the image. After the map is computed, a

user manually selects two seed points indicating the extremities of the segment of interest. Finally, a connected centerline between the points was found using a minimum cost algorithm for the map computed earlier. The results were presented through the measuring distance between manually determined ground truth path and the path produced by the algorithm for fifteen coronary artery segments. The best configuration of the algorithm resulted in the maximum distance of 3.85 mm while the worst average distance was 1.53 mm.

Another global optimization approach is described in Li and Yezzi [2007], where the vessels were modeled as four-dimensional entities. The basic idea here was to take the three-dimensional image and transform it to a four-dimensional cost space with three spatial dimensions and one more scale dimension. Each point in this space is the scalar that is inversely proportional to the likelihood of this point being a sphere that fits the vessel of the appropriate size. Then, given the start and the end seed points in the cost space, one may find the path between them that minimizes the total cost. A fast marching method was applied to solve the optimization problem. The quantitative analysis was done on five cardiac CTA cased based on volumetric comparison of ground truth and algorithmic segmentation. Correct segmentation (true positive) fraction varied from 42.5% to 75.2%. Oversegmentation (false positive) fraction varied from 30.7% to 91.9%.

The main difference in these categories of optimization is in the ability to incorporate the knowledge of local and global behavior of the blood vessel. For example, a local method may have the strength of careful modeling of sharp artery turns but, at the same time, would be unable to jump over large disconti-

nuity. A global method would produce a path for the artery from the start point to the end point, but local windings may not be modeled properly which would lead to low path accuracy.

The remaining part of this thesis gives the detailed description of the method used for coronary artery modeling and reconstruction, experimental setup and obtained results. The last section contains discussion of the results and possible extensions to this work.

CHAPTER 2

# THE ARTERY RECONSTRUCTION METHOD

In this chapter the method of extracting coronary artery centerlines from CTA images is introduced. First, the very general geometrical model for blood vessel is described. Then this model is refined and modified to fit the particular features of the coronary artery and CTA imaging modality. Finally, the algorithm of matching the constructed model to a particular CTA image is presented.

## 2.1 General model

An image of coronary artery lumen may be represented by a connected set of cylindrical components each having a unique location, size and orientation. An illustration for such a model is given in Figure 2.1. Further we propose a technique for determining the parameters of this model given a starting seed point located at on end of the vessel and an initial direction.

Our method is based on the assumption, that one can construct a distinct volumetric model $M$ of the blood vessel given its three-dimensional digital image $S$. The model construction process can be seen as an optimization in which we look for the model $M_k$ consisting of multiple components $\{t_i\}_k$ that will result in maximized sum of local similarity measures $\rho(t_i, S)$ computed over each individual component:

$$M_{max} = \arg\max_{\{t_i\}_k} \sum_i \rho(t_i, S). \tag{2.1}$$

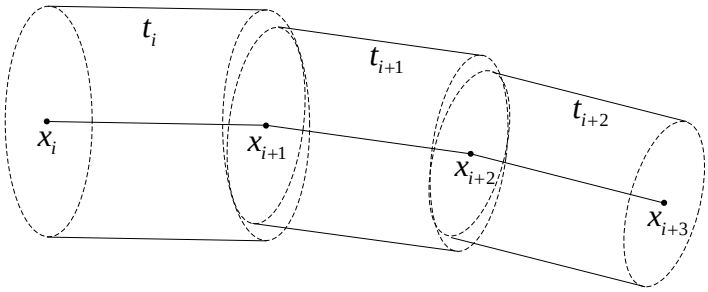


Figure 2.1: An example of multiple component model of coronary artery. The body of the vessel is split into multiple segments, where each one is parameterized individually and independently from other segments.

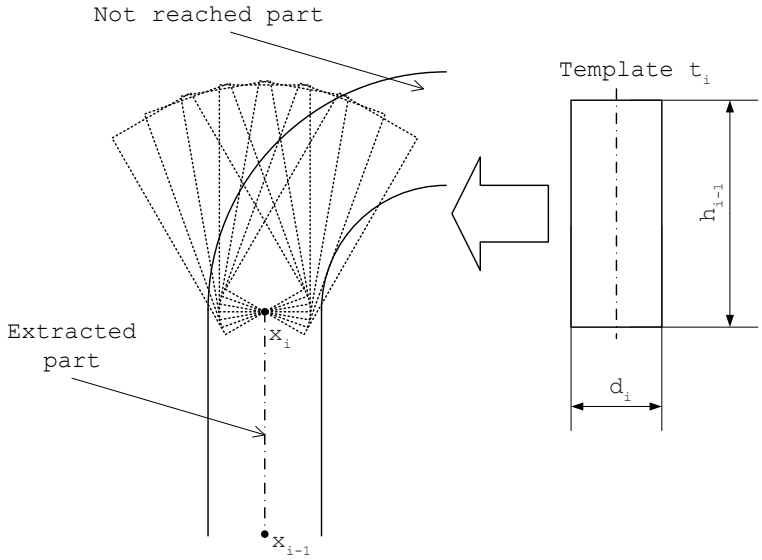


Figure 2.2: Search for the model template that best describes a segment of the artery.

In this work we explore the case, when optimization is accomplished for one single segment at a time, that allows finding optimal solution locally. We search through the space of parameters describing an artery segment until we have found the one that would fit image data the best. The results of optimization are then frozen and used as the initial condition for the next segment optimization and so on as depicted in Figure 2.2.

## 2.2 Model constraints

Considering some important properties of coronary arteries we may impose certain constraints on the model that will allow us to build less generalized but still good representation of the blood vessel. At the same time the search space for optimal template search is being reduced. The following are the set of the constraints derived from the general properties of coronary artery.

First, the set of all possible three-dimensional spatial curves describing the centerline can be reduced to splines of order one (set of piecewise linear segments). Here the curve can be defined by the finite set of the knot points $\{x_i\}$, assuming that the centerline is a straight line in between. By varying the segment distance $h_i$ between subsequent points of the centerline, we can change the "resolution" of the curve and make it arbitrarily smoother or coarser. Splines of higher order, such as quadratic or cubic, may also be used, however they introduce additional degrees of freedom to the model which is undesirable as is explained above.

Second restriction comes from the notion of the roundness of a typical blood vessel's profile. If we assume, that the diameter of the vessel does not vary much locally, we can represent its shape as a solid cylinder of fixed diameter $d_i$ having the centerline segment $x_i\, x_{i+1}$ as its axis. This way the entire artery can be approximated by a chain of cylinders $\{t_i\}$ stitched together.

General optimization approach outlined above assumes the search of single segment model parameters, given that the end point and orientation of neigh-

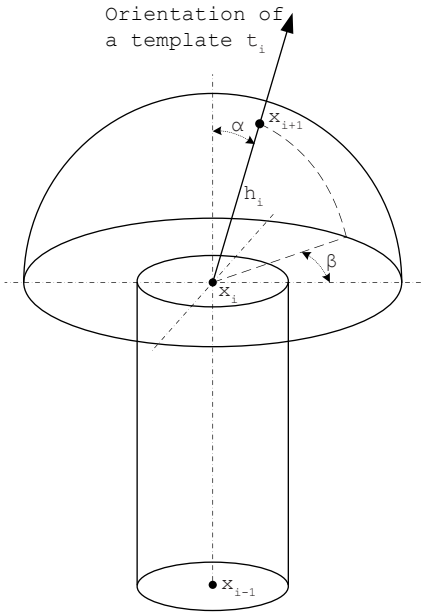


Figure 2.3: Specifying direction: $\alpha$ (zenith) and $\beta$ (azimuth) determine the orientation of a template $t_i$ in space relative to $t_{i-1}$.

boring segment are already known. Geometrically, individual cylindrical template $t_i$ may be defined by the start point, the end point and the diameter. It is easier to make a reparameterization using angular coordinates (distance, zenith, azimuth), i.e. instead of specifying the coordinates of its end point $x_{i+1}$ explicitly, we specify the length of the segment and the angular deviation with respect to the orientation of the previous segment.

Third, given that bend of a coronary artery is limited, for two sequential segments $x_{i-1}\, x_i$ and $x_i\, x_{i+1}$ we add maximum curvature (maximum zenith angle $\alpha_{max}$) constraint that limit spatial co-location of three subsequent knot points of the centerline:

$$\alpha_i = \angle(x_{i-1}\, x_i,\ x_i\, x_{i+1}) < \alpha_{max} \tag{2.2}$$

In this formulation, the end point $x_{i+1}$ of the segment lies within a spherical cap

of the cone defined by its generatrix length $h_i$ and the maximum zenith angle $\alpha_{max}$ as displayed in Figure 2.3.

Fourth, we fix the aspect ratio $r_a$ of template height to its diameter and optimize for the diameter only. Consequently thicker segments of the artery will be modeled with the templates of greater lengths:

$$h_i = r_a d_i. \tag{2.3}$$

There is a very important trade off, associated with choosing the value of $r_a$. On one hand, the higher is the aspect ratio, the longer is the template, and therefore more image information is used in the matching procedure. Consequently the algorithm will more likely to overcome discontinuities and lumen shape abnormalities. On another hand, shorter templates allow for more precise modeling of a coronary artery bending and, most likely, would result in smaller reconstruction error.

Fifth, anatomically it is impossible for an artery to change its diameter drastically between two adjacent segments; therefore we may limit diameter search space as well:

$$d_i \in [\delta_{\min} \cdot d_{i-1}, \delta_{\max} \cdot d_{i-1}], \tag{2.4}$$

where $\delta_{\min} < 1.0$ and $\delta_{\max} > 1.0$ are predefined coefficients that limit change in diameter relatively to the previous segment. This constraint is also useful in detecting coronary artery junction point with the aorta and is explained later.

Now we can easily see that position of knot points $x_{i-1}$, $x_i$, template diameter $d_i$, zenith $\alpha_i$, azimuth $\beta_i$ entirely determine position of the template and subsequent knot point $x_{i+1}$. Realizing that $x_{i-1}$ and $x_i$ are known from previously

found segment, only three parameters define the geometry of the current segment model.

## 2.3 Model-image similarity criterion

The local model-image similarity measure $\rho(t_i, S)$ should result in a maximum positive response when a template is imposed exactly over the coronary artery and in smaller response otherwise. Provided that the contrast medium is distributed uniformly in the blood, the image intensity of the voxels corresponding to the lumen is higher than the intensity of surrounding space. This feature helps human reader visually distinguish a coronary artery from a contrast enhanced CT image. The similarity measure should neither be affected by the change in contrast material density, nor by presence of the high-intensity calcified plaque, therefore local intensity threshold $I_i$ is used in its formulation. If we denote $V(t_i, I_i)$ to be the volume of the image $S$ having intensity above $I_i$ enclosed in the template $t_i$ and $V(t_i)$ to be the volume of the template itself, then we may define the measure as the fraction:

$$\rho_{I_i}(t_i, S) = \frac{V(t_i, I_i)}{V(t_i)}. \tag{2.5}$$

Here $t_i$ is the cylindrical template, that determined both by its geometrical properties and intensity threshold. By applying this measure, we choose the template orientation such that it has as much high intensity volume enclosed into it as possible. The intensity threshold is not a global parameter: it may change its value depending on the local intensity of the lumen that may vary depending on concentration of contrast medium. Flexible thresholding scheme, described

in algorithm section, also allows to account for partial volume effect that especially affects the intensity of narrow vessels.

The local intensity threshold range is limited:

$$I_i \in [I(x_i) - I_{drop}, I_{max}], \tag{2.6}$$

where $I(x_i)$ is the vessel image intensity at knot point $x_i$, $I_{drop}$ is the predefined maximum negative change of intensity and $I_{max}$ is the absolute maximum intensity threshold.

In order to account for the image noise and possible gaps in artery continuity, we allow a partial match, i.e. $\rho_{I_i}(t_i, S)$ may be less than 1. We consider that template is matched the image if the following match criterion is satisfied:

$$\rho_{I_i}(t_i, S) > P, \tag{2.7}$$

where $P$ is the template match threshold. One may notice, that with $I_i$ small enough there are a lot of possible geometrical orientations of a template that would result in $\rho_{I_i}(t_i, S) = 1$ or absolute match. Thus $I_i$ must be high enough, such that only single geometrical instance of the template $t_i$ satisfies the match criteria.

One may notice that the similarity criterion depends only on the local image intensity information and no anatomical knowledge on possible position or orientation of coronary artery is used. In other words, the algorithm does not have the information about expected direction of the centerline path in advance. This is fundamental assumption of the method which makes it only suitable for processing of CTA images where the coronary arteries are enhanced by the contrast

medium. Images that are too noisy or have poor contrast would be extremely challenging for such a method.

## 2.4 The artery reconstruction algorithm

Implementation of the sequential optimization with all the constraints described previously is shown in Figure 2.4. The main components of the algorithm, initialization, matching and model adjustment are described in details further in this section.

Since tracking algorithm always needs a previous segment location and orientation to proceed, the very first segment must be initialized manually. In order to do that, a user must specify two seed points $x_0$ and $x_1$ within the artery corresponding to the first segment of the spline. From the algorithmic point of view it does not matter in which direction an artery is tracked, however if it is done from the aortic origin toward myocardium, there is ambiguity at the bifurcation points: both branches may lie within spherical cone and the algorithm would pick a random path. To avoid this situation, the algorithm is seeded in opposite direction - toward the aorta: accordingly the artery is traced against the blood flow direction and vessel bifurcations are not the issue. Another question is how far from aorta the first segment should be. The segments that are far away from their aortic origin are very small in diameter and are very hard to identify even by looking at the image: even if they had the disease, one would not be able to evaluate it using CTA image. Thus as a start point we pick the healthy segment, that is clearly distinguishable from the background and has at

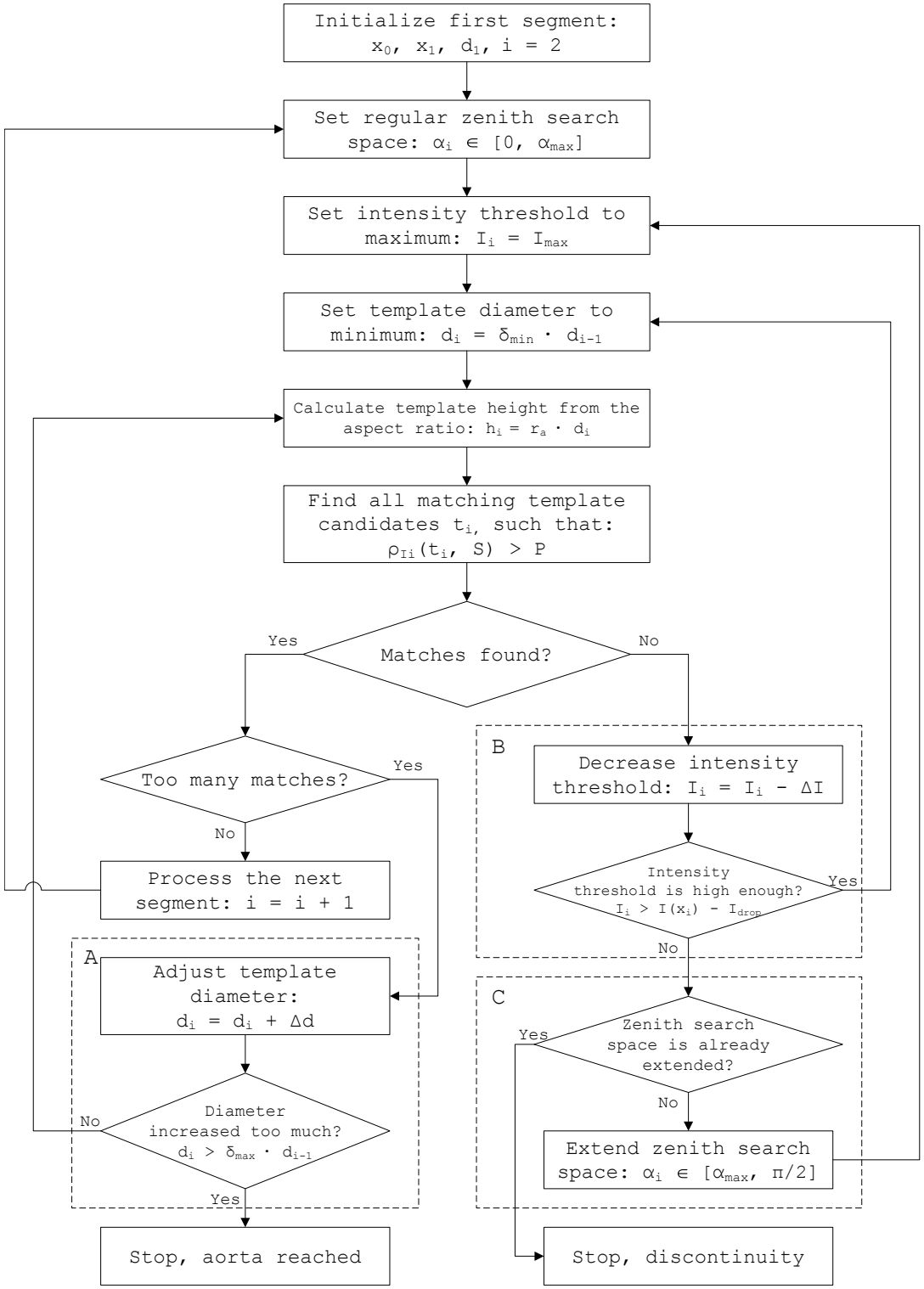


Figure 2.4: Algorithm scheme for an individual artery centerline extraction

least two to three voxels in diameter (about 1 - 1.5 mm thickness for the experimental images). This way the diameter of the first segment was always about the same and there was no requirement for a user to specify it.

Once the first segment is initialized by user and the search parameters are set to their default values, the optimization of the model's free parameters begins. For each permitted pair of direction angles $(\alpha_i, \beta_i)$, the corresponding cylindrical template $t_i$ is constructed on top of already extracted artery segment and model-image similarity metrics $\rho_{I_i}(t_i, S)$ is calculated. The space of possible angle pairs was discretized with the intervals of $\alpha_{step}$ and $\beta_{step}$ for zenith and azimuth respectively. The process of constructing a template involves generation of a local image mask consisting of the voxels, whose centers lie within the volume of the cylinder. In order to obtain the numerical value of the similarity measure, the volume of high intensity image voxels above the intensity threshold within the mask is divided by the total volume of the mask. Here it is crucial to consider image anisotropy and use physical coordinates for proper geometrical modeling of the cylinder. In order to speed-up the optimization process, it is recommended to have the all possible templates with different orientations and size precomputed and stored in operating memory repository.

After all templates are generated and corresponding matching metrics are found, the subset of templates satisfying (2.7) is selected. Based on the number of matches remaining, the algorithm decides how to proceed.

The procedure of automatic diameter adjustment is depicted in Figure 2.4, section A. If the size of this subset is greater than one, it corresponds to the sit-

uation when multiple templates with different orientation fit the image data. It usually means that the diameter of coronary artery has increased and the template has not been adjusted accordingly. Therefore, the diameter of the template must be increased while the intensity threshold is kept at the same level. Then the search procedure is repeated until only a single template is left in this subset. This template becomes the best match of the model and the part of the extracted part of the artery. Sometimes with the increase of the template diameter, all matches disappear. It happens because of discrete character of the change in diameter and the corresponding image mask used in the matching procedure. In this case, the best matching template found in the previous step is used.

The procedure of automatic intensity threshold adjustment is shown in Figure 2.4, section B. Sometimes, not a single template may match the image. This, for instance, may happen in case of the sudden drop of vessel intensity. Here the intensity threshold must be decreased to accommodate this change until a matching template is found. Again, in software implementation decrease of intensity threshold is discrete and therefore number of matched templates could jump steeply from zero to a certain number. In this case the template with highest $\rho_{I_i}(t_i, S)$ is considered to be the matching one. If the threshold drops below the certain level and the match is still not found, it is likely that the severe discontinuity is reached.

The procedure of automatic angular search space adjustment corresponds to the section C in Figure 2.4. Another reason why the matching template may not be found could be an unusually sharp turn caused either by a natural artery bend or the stairstep artifact. In this case zenith search space is extended up and

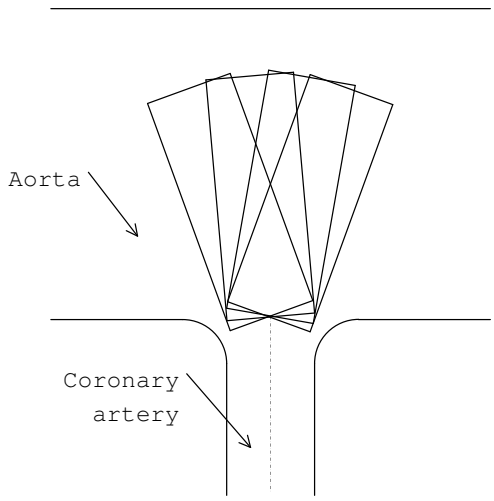


Figure 2.5: Too many matching templates is a good indication that the aorta has been reached.

matching procedure is repeated again.

In summary, extraction of a single segment of the artery generally involves the optimization for two angles specifying direction of the template. In certain circumstances, the optimization of the template's size and intensity threshold is also necessary.

The algorithm has two main termination conditions. First condition means that tracking process reached discontinuity that cannot be overcome by standard means of decreasing the intensity threshold and extending angular search space. In this case the algorithm must be reseeded at the point where it stopped. Second condition means that the tracking process reached aorta. This happens when the vessel diameter jumps relative to the previous segment by a factor exceeding $\delta_{\max}$ as illustrated in Figure 2.5. In addition to these two conditions, the algorithm is stopped, when the best matching segment hits already extracted artery branch.

CHAPTER 3

# EXPERIMENTAL SETUP AND ALGORITHM VALIDATION

## 3.1 Dataset description

In this study we used twelve cardiac CTA cases, where each case corresponds to a single patient. Each case contained multiple three-dimensional images with the parameters shown in Table 3.1. For each case image datasets were retrospectively reconstructed at twenty consecutive phases of the cardiac cycle. In order to minimize the impact of cardiac motion and reconstruction artifacts on the algorithm, only a single image, most relaxed, state of the heart, was chosen for each case. It was selected manually by visual examination of the dataset and assessing the degree of motion blur and severity of stairstep artifacts for every image. For each selected image, the left anterior descending artery (LAD), the right coronary artery (RCA), left circumflex artery (LCX), and the first diagonal branch of LAD (DIAG) were identified and seed points were manually located as described in previous chapter.

## 3.2 Validation criteria

The quality of the algorithm was evaluated using two criteria: (a) the portion of the artery, traced from a single manual initialization (sensitivity) and (b) the geometrical accuracy of the reconstruction.

Table 3.1: Image and scanner parameters

| | |
|---|---|
| Axial image size | 512x512 |
| Slice thickness | 0.625 mm |
| In-plane resolution | 0.48 ... 0.52 mm |
| Contrast medium | Visipaque 320 |
| CT Scanner model | GE LightSpeed VCT |
| Year of manufacture | 2004 |
| Number of channels | 64 |
| Gantry revolution time | $\geq$ 0.35 s. |
| Beam | 120 kVp, 700 mA (approx.) |
| Additional feature | Built-in motion artifact reduction |

The portion of the artery automatically extracted from a single initialization, or sensitivity, is an important characteristic of the method and indicates the amount of additional work the operator has to do to complete the analysis. If the method failed to complete the reconstruction of the specified branch, it was reseeded and started again at the point where the fail occurred. After the remaining portion of the artery was reconstructed, the length of the first reconstructed segment prior to the failure was divided by the total length of the branch and the ratio was recorded. All available artery branches were evaluated using this criterion.

The second criterion, the accuracy, can be expressed as the mean and maximum distance between automatically and the manually marked centerlines. In order to obtain this measure, two independent observers were asked to mark

the centerlines using the 3D image annotation tool. Before computing these measures, automatically extracted segments were visualized and inspected to ensure their topological validity. In order to compute the distances between the centerlines, the measures similar to asymetric chamfer and Hausdorff metrics were used. If denote $X = \{x_i\}_{i=0,M}$ as automatically and $Y = \left\{y_j\right\}_{j=0,N}$ as manually marked set of centerline knot points, then we can express the measured distances as the following:

$$D_{mean}(X,Y) = \frac{1}{M}\sum_i \min_j d\left(x_i, y_j y_{j+1}\right), \tag{3.1}$$

$$D_{max}(X,Y) = \max_i \min_j d\left(x_i, y_j y_{j+1}\right), \tag{3.2}$$

where $d\left(x_i, y_j y_{j+1}\right)$ is the closest Euclidean distance between the point $x_i$ and the segment $y_j y_{j+1}$. More specifically, for each segment of $X$ the closest point belonging to $Y$ is found and the distance is calculated. The final value of the first metric is simply this distance averaged for all segments of $X$. In this regard, $D_{mean}$ is the same metric suggested by Olabarriaga et al. [2003] for assessing the accuracy of reconstructed artery from CTA image. This measure equals to the average distance between two splines comprised of multiple line segments. The final value of the second metric is the maximum among all these distances. It measures the extent of the largest gap between automatically and manually marked centerlines. These metrics were computed for five LAD arteries for which manual delineations were done.

## 3.3 System training (parameter optimization)

As follows from Section 2.4, the algorithm for artery reconstruction has two functionally different sets of parameters: dynamic and static. The dynamic set of runtime parameters is obbtained based on the results of the most recently processed segment. These parameters are of zenith $\alpha_i$ and azimuth $\beta_i$ angles, the template diameter $d_i$ and the intensity threshold for matching metric $I_i$. The static parameters (listed in Table 3.2) were determined empirically by algorithm optimization on a set of training cases.

In order to determine the values of static parameters, the experiments with two different LAD arteries (cases CU0001, CU0017) were done. These two cases were selected because of the great amount of bends and extent of stairstep artifacts respectively. Several runs with various set of variables were done. Because of the adaptive nature of the algorithm, different values resulted in very similar outcomes, with the only difference in the running time.

The parameter that had the greatest effect on the outcome of the centerline reconstruction was the aspect ratio $r_a$ for the template. With smaller values (short cylinder), the ”resolution” of the centerline was high, and sharp bends of the lumen could be processed with very high accuracy. However, due to the reasons mentioned in Section 2.2, short templates capture a little of the image information. They tend to align with random noisy voxels near the lumen and are unable to ”jump” over intensity gaps and discontinuities caused by stairstep artifact. Higher values of $r_a$ (longer cylinders), were more tolerant to these issues, however, the accuracy on the artery turns was significantly reduced. The

Table 3.2: Static parameters of the algorithm

| Parameter | Value | Description |
|---|---|---|
| $\delta_{min}$ | 0.75 | Minimum diameter decrease coefficient |
| $\delta_{max}$ | 1.50 | Maximum diameter increase coefficient |
| $\Delta d$ | 0.1 | Radius increment |
| $\alpha_{max}$ | $\pi/4$ rad | Limiting angle for zenith search space |
| $\alpha_{step}$ | $\pi/16$ rad | Step for zenith angle |
| $\beta_{step}$ | $\pi/6$ rad | Step for azimuth angle |
| $r_a$ | 5.0 | Template height/diameter aspect ratio |
| $I_{max}$ | 200 HU | Maximum intensity threshold for template |
| $I_{drop}$ | 30 HU | Maximum intensity threshold difference between adjacent templates |
| $\Delta I$ | 10 HU | Intensity decrement |
| P | 0.95 | Match criterion threshold |

combination of high $r_a$ values and sharp artery bend could result in an inability of the algorithm to follow a sharp turn and its premature termination as a result. Given these considerations, the smallest possible value of $r_a$ that allowed processing both cases with a sensitivity of 1.0 was found. The value of $r_a$ = 5.0, slightly greater than the found value, was used as the final parameter of the algorithm.

The rest of the static parameters were not separately optimized. With the limited number of training cases, such optimization could have forced the

model to overfit and generalize poorly. Instead, these parameters were set up to the reasonable values with additional small safety margins that allowed to process both training segments in time less than three minutes each. The values of these constants are shown in the table.

Parameters $\delta_{min}$ and $\delta_{max}$ determine the minimum and maximum ratios of diameters for the adjacent segments. Such ratio was initially defined to be not greater than 25%. However, the diameter of the artery has a tendency to increase as the tracing proceeds towards the aorta, so the current segment is allowed to be additional 25% thicker that the previously extracted one. The diameter increase step is selected to be 0.1 mm, because with the fixed aspect ratio, the length of the template would increase by 0.5 mm which roughly equals the voxel spacing of the experimental images. The larger ratios and smaller steps are unnecessary, and would only increase the dynamic optimization time.

Limiting angle for zenith search space is set to be $\pi/4$ rad, so that the direction of the artery is preserved relative to the previous step. Lower values would require shorter templates to accomodate for sharp turs, while larger values would increase the search time and, possibly, create a hazard of following the wrong artery branch. Step for zenith angle $\alpha_{step}$ is selected as $\pi/16$ rad to allow finer search within the osculating plane. Step for azimuth angle is $\pi/6$ is much coarser, since the torsion of the centerline is limited. Finer values would work, however the dynamic search time will be increased as well.

The intensity of large healthy coronary arteries enhanced by contrast was ranging from about 200 to 400 HU depending on the case. The images of nar-

rower arteries might have much lower intensities due to partial volutme effect. For this reason the threshold for model-image similarity criterion was set up to start from the value of 200 HU and decreased gradually with the step of 10 HU. The maximum absolute difference in threshold between adjacent templates was selected to be 30HU. This was done to detect large discontinuity to prevent the artery from aligning with a noisy cluster of bright voxels. With larger values may force the algorithm to align with random bright voxels at the discontinuity point.

Match criterion threshold $P$ of 0.95 was selected to be close to 1, with a margin of 5% to allow for partial segment match due to possibility of having few noisy low-intensity noisy voxels within the segment volume.

CHAPTER 4

# RESULTS AND CONCLUSIONS

An example of automatically extracted centerline for one of the cases together with manual markings is shown in Figure 4.1. Black circles represent the markings created by our automatic method and gray circles represent the manual marks. The diameter of each circle is 1 mm. Also, the result of the artery traversing can be represented as a chain of best fitting cylindrical templates connected together as shown in Figure 4.2. The connected set of cylindrical templates superimposed to the image of the heart is shown in Figure 4.3.

## 4.1 Quantitative evaluation

The sensitivity, or the ratios of automatically extracted segment to visually discernible artery lengths, are shown in Table 4.1. As we can see, for 40 out of 47 vessels, the algorithm identified the entire length of the artery branch with a single manual initialization. In addition, the method was able to track arteries containing calcifications and surgical stents as showed in Figure 4.4.

Figure 4.1: Same segment of the artery: comparison of automatically (black) and manually (gray) marked axis (diameter of each circle is 1mm)

Figure 4.2: Modeled segment of LAD (20% of full length is shown): cylinders of different shades represent best matching templates stitched together

Figure 4.3: Volume rendering of the heart region with RCA and LAD represented as piece-wise cylinder tubes (marked white). Diameter of the the cylinders is increased for visualization purposes.

Table 4.2 shows the geometrical accuracy as maximum and mean difference between manually and automatically marked segments. In all cases the algorithm was able to reconstruct the central axis within the mean distance of 0.70 mm and the maximum distance of 2.15 mm between the segments.

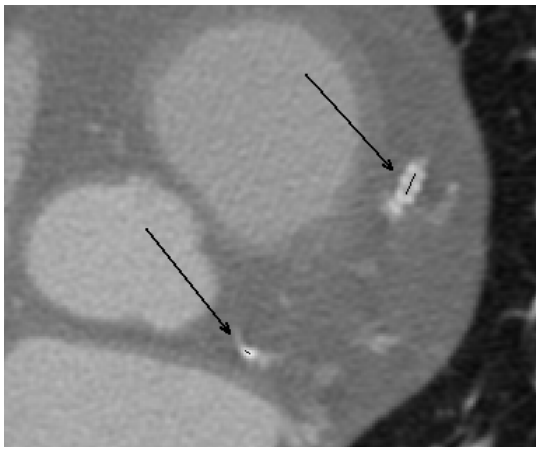

Figure 4.4: A CTA slice showing the segment of centerline (thin black line) extracted from the calcified portion of the LCX artery (bottom arrow) and the centerline passing through the stent at LAD artery (top arrow).

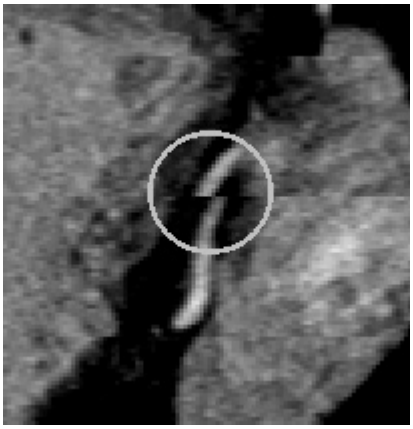

Figure 4.5: CX0017, RCA: Example of the case with premature completion due to significant discontinuity caused by stairstep artifact.

## 4.2 Failure cases

In four out of seven cases of premature completion, the algorithm stopped at a point of stairstep discontinuity caused by cardiac motion, an example of which is shown in Figure 4.5. In the case CX0017 (LCX), the algorithm incorrectly identified the tangent boundary of the heart as the junction point with the aorta

Table 4.1: Portions of artery branches extracted from a single manual initialization.

| Case | Branch | | | |
|---|---|---|---|---|
| | LAD | RCA | LCX | DIAG |
| CX0001 | 1.0[1] | 1.0 | 0.3 | 1.0 |
| CX0017 | 1.0[1] | 0.3 | 0.2 | 1.0 |
| CX0018 | 1.0 | 1.0 | 1.0 | 1.0 |
| CX0019 | 1.0 | 1.0 | 1.0 | 1.0 |
| CX0020 | 1.0 | 1.0 | 0.9 | 0.6 |
| CX0021 | 0.2 | 1.0 | 1.0 | 1.0 |
| CX0023 | 1.0 | 1.0 | 1.0 | 1.0 |
| CX0030 | 1.0 | 1.0 | 1.0 | 1.0 |
| CX0031 | 1.0 | 0.2 | 1.0 | 1.0 |
| CX0032 | 1.0 | 1.0 | - | 1.0 |
| CX0034 | 1.0 | 1.0 | 1.0 | 1.0 |
| CX0035 | 1.0 | 1.0 | 1.0 | 1.0 |

[1] artery was used for training

as shown in Figure 4.6.

In case CX0021, the quality of the image was seriously affected by heart motion and the image of the artery was not clearly visible along its length. In case CX0031 the tracking process made the wrong turn toward another branch of RCA artery (in this case the algorithm was stopped manually). In all these cases, the algorithm could be manually reseeded from the point where it stopped, and when this was done, it was able to complete the delineation procedure.

Table 4.2: Maximum and mean distances between automatically and manually marked centerlines

| | | Distance between automatic and manual markings, mm | | | |
|---|---|---|---|---|---|
| | | Automatic - Observer 1 | | Automatic - Observer 2 | |
| Case | Length, mm | max | mean | max | mean |
| CX0001[1] | 148 | 2.15 | 0.69 | 2.15 | 0.53 |
| CX0017[1] | 153 | 1.27 | 0.53 | 1.17 | 0.57 |
| CX0018 | 127 | 1.41 | 0.58 | 0.65 | 0.37 |
| CX0019 | 151 | 1.11 | 0.55 | 1.42 | 0.61 |
| CX0020 | 150 | 1.83 | 0.64 | 2.01 | 0.69 |
| Average | | | 0.60 | | 0.55 |

[1] artery was used for training

## 4.3 Conclusions and possible extensions

An automated method that can extract the central axes of the coronary arteries from CTA images has been presented in this thesis. Results obtained in this work indicate that the method can be used to approach this goal. The algorithm was specifically designed to handle coronary arteries that can be affected by noise, heart motion and image reconstruction artifacts. The cylinder modeling approach allowed us to extract even very thin artery segments that can be seen on a CTA image. Because of the flexibility and adaptive nature of the algorithm, it has the ability to track arteries of different sizes and curvatures, containing calcifications and surgical stents. The template matching scheme could even tolerate certain degree of stairstep artifacts by preserving the orientation of the

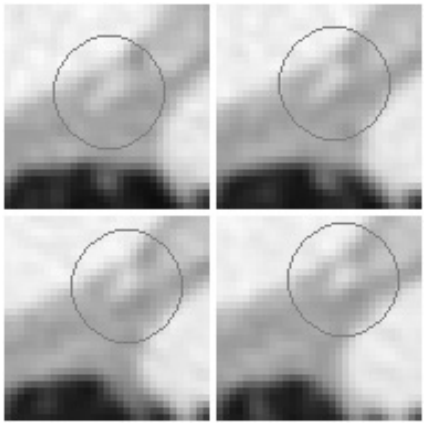

Figure 4.6: CX0017, LCX: Significant drop of image intensity nearby one of the heart chambers. Algorithm erroneously decides that aorta is reached.

vessel. The method requires minimum user interaction and was able to extract the centerline automatically with both high sensitivity and geometrical accuracy: for 85% branches, the algorithm was able to reconstruct the entire centerline from a single initialization and the average distance between the automatic and manual markings did not exceed 0.70 mm with the maximum distance of 2.15 mm.

Among major limitations of the method are inability to overcome large stairstep artifacts and poor performance on blurry images, affected by heart motion. Another restriction is that the lumen of coronary artery has to be at least two to three voxels in diameter, so that the template optimization is able to establish a reliable match with the image data. If the artery is diseased and there is a soft plaque on its inner walls, the presented method would identify only the centerline of the lumen, but not the artery itself.

There are possible extensions to the suggested scheme that could lead to

higher applicability and efficiency of the algorithm. These extensions are related either to the minimization of user interaction or to the increase in accuracy of the algorithm.

The burden on the operator can be reduced if the image corresponding to the proper phase of the cardiac cycle is selected automatically. This can be done by estimating amount of cardiac motion or severity of stairstep artifacts. Automated selection of seed points can also be used: most likely, it will require incorporating certain anatomical knowledge about the geometric origin of the arteries into the algorithm.

The speed of the reconstruction can be improved by employing the knowledge about position of coronary arteries relative to the heart. Provided that the heart is segmented by another algorithm, spatial constraints can be imposed on the reconstruction. Consequently, the effectiveness of the search will be improved.

More flexible template shape may be used to increase the accuracy of the reconstruction at the sharp turns. Cylindrical templates, while simple and efficient, are not suitable for modelling very sharp artery turns. One solution would be to use two shorter templates connected together and optimize both of them at each iteration to allow for more flexibility. Another solution would be to model an artery centerline by a spline of a higher order. Both solutions are likely to increase the accuracy of the algorithm, but indeed, computational cost will also be increased.

Finally, a combination of global and local optimization may be used to overcome the problems introduced by local defects of the image such as intensity gap, motion blur or stairstep artifact. The main purpose of the global method would be to define the approximate location of the centerline path, while the local method would validate and refine this path locally.

## BIBLIOGRAPHY


D. P. T. Banh, I. S. Kyprianou, S. Paquerault, and K. J. Myers. Morphology-based three-dimensional segmentation of coronary artery tree from CTA scans. In *Proceedings of SPIE*, volume 6512, page 65122I, 2007.

H. Blum. A transformation for extracting new descriptors of shape. *Models for the Perception of Speech and Visual Form*, pages 362–380, 1967.

C. Boldak. *Extraction et caracterisation 3D des reseaux vasculaires en imagerie scanner multibarette: Application aux reseaux des membres inferieurs et des coronaires*. PhD thesis, Universite de Rennes, 2003.

K. Bühler, P. Felkel, and A. La Cruz. Geometric Methods for Vessel Visualization and Quantification - A Survey. *Geometric Modelling for Scientific Visualization*, pages 399–420, 2003.

J. Dehmeshki, X. Ye, H. Amin, M. Abaei, X. Li, and S. D. Qanadli. Volumetric Quantification of Atherosclerotic Plaque in CT Considering Partial Volume Effect. *IEEE Trans. Med. Imaging*, 26(3):273–282, 2007.

C. Kirbas and F. Quek. A Review of Vessel Extraction Techniques and Algorithms. *Computing surveys*, 36(2):81–121, 2004.

A. F. Kopp, A. Kuttner, T. Trabold, M. Heuschmid, S. Schroder, and C. D. Claussen. Multislice CT in cardiac and coronary angiography. *British Journal of Radiology*, 77:S87–S97, 2004.

K. Krissian, G. Malandain, N. Ayache, R. Vaillant, and Y. Trousset. Model-based detection of tubular structures in 3D images. *Computer Vision and Image Understanding*, 80(2):130–171, 2000.

L. Lam, S. W. Lee, and C. Y. Suen. Thinning methodologies-a comprehensive survey. *Pattern Analysis and Machine Intelligence, IEEE Transactions on*, 14(9): 869–885, 1992.

G. Lavi, J. Lessick, P. C. Johnson, and D. Khullar. Single-seeded coronary artery tracking in CT angiography. In *Nuclear Science Symposium Conference Record*, volume 5, pages 3308–3311, 2004.

L. P. Lawler, H. K. Pannu, and E. K. Fishman. MDCT evaluation of the coronary arteries, 2004: how we do it–data acquisition, postprocessing, display, and interpretation. *American Journal of Roentgenology*, 184(5):1402–12, 2005.

H. Li and A. Yezzi. Vessels as 4-D Curves: Global Minimal 4-D Paths to Extract 3-D Tubular Surfaces and Centerlines. *IEEE Trans. Med. Imaging*, 26(9):1213–1223, 2007.

D. Maintz, M. Gride, E. M. Fallenberg, W. Heindel, and R. Fischbach. Assessment of coronary arterial stents by multislice-CT angiography. *Acta Radiologica*, 44(6):597–603, 2003.

C. Metz, M. Schaap, A. Van Der Giessen, T. Van Walsum, and W. Niessen. Semi-automatic coronary artery centerline extraction in computed tomography angiography data. In *4th IEEE International Symposium on Biomedical Imaging: From Nano to Macro*, pages 856–859, 2007.

D. Mueller, A. Maeder, and P. O'Shea. Improved Direct Volume Visualisation of the Coronary Arteries Using Fused Segmented Regions. In *IEEE DICTA: Proceedings of the Digital Image Computing on Techniques and Applications*, page 17, 2005.

S. Olabarriaga, M. D. Breeuwer, and W. J. Niessen. Minimum Cost Path Algorithm for Coronary Artery Central Axis Tracking in CT Images. *Lecture notes in computer science*, pages 687–694, 2003.

S. Schroeder, A. F. Kopp, B. Ohnesorge, H. Loke-Gie, A. Kuettner, A. Baumbach, C. Herdeg, C. D. Claussen, and K. R. Karsch. Virtual coronary angioscopy using multislice computed tomography. *Heart*, 87(3):205–209, 2002.

B. H. Thompson and W. Stanford. Update on using coronary calcium screening by computed tomography to measure risk for coronary heart disease. *The International Journal of Cardiovascular Imaging*, 21(1):39–53, 2005.

J. A. Tyrrell, E. di Tomaso, D. Fuja, R. Tong, K. Kozak, R. K. Jain, and B. Roysam. Robust 3-D Modeling of Vasculature Imagery Using Superellipsoids. *IEEE Trans. Med. Imaging*, 26(2):223–237, 2007.

P. M. A. van Ooijen, G. de Jonge, and M. Oudkerk. Coronary fly-through or virtual angioscopy using dual-source MDCT data. *European Radiology*, 17(11): 2852–2859, 2007.

O. Wink, Wiro J. Niessen, and M. A. Viergever. Fast Delineation and Visualization of Vessels in 3D Angiographic Images. *IEEE Trans. Med. Imaging*, 19(4): 337–346, 2000.

W. C. K. Wong and A. C. S. Chung. Augmented Vessels for Quantitative Analysis of Vascular Abnormalities and Endovascular Treatment Planning. *IEEE Trans. Med. Imaging*, 24(6):665–684, 2006.

Y. Yang. *Image segmentation and shape analysis of blood vessels with applications to coronary atherosclerosis*. PhD thesis, Georgia Institute of Technology, 2007.

Z. Ye, Z. Lin, and C. C. Lu. A fast 3D region growing approach for CT angiography applications. In *Proceedings of SPIE*, volume 5370, pages 1650–1657, 2004.

P. J. Yim, J. J. Cebral, R. Mullick, H. B. Marcos, and P. L. Choykel. Vessel Surface Reconstruction With a Tubular Deformable Model. *IEEE Trans. Med. Imaging*, 20(12):1411–1421, 2001.